Journal of
Applied Crystallography
ISSN 0021-8898

Received 18 July 2003
Accepted 25 May 2004

Depth capabilities of neutron and synchrotron diffraction strain measurement instruments. II. Practical implications

Philip John Withers

Manchester Materials Science Centre, Grosvenor Street, Manchester M1 7HS, UK. Correspondence e-mail: philip.withers@man.ac.uk

In part I [Withers (2004). *J. Appl. Cryst.* **37**, 596–606], a framework was presented for estimating the maximum feasible penetration length for neutron and synchrotron X-ray strain measurement. This calculation reflected the attenuation and scattering capability of the material under examination, the incident flux and detector arrangement, the likely background signal, the required strain measurement accuracy, the sampling volume, and the diffracting geometry. In the present paper (part II), preliminary calibration data acquired for a very wide range of neutron and synchrotron sources are presented. This database is used to explore the implications of the framework for delineating those conditions under which a specific instrument can provide useful information within a feasible timescale, in order to identify the most appropriate radiation, energy and instrumental configuration for undertaking measurements in transmission and reflection as a function of depth, and to establish guiding principles for improving the performance of existing instruments.

1. Introduction

Large-scale neutron and synchrotron X-ray facilities are finding increasing application for the measurement of strain at depth in engineering components. The prime advantage of these methods over laboratory X-ray methods is the ability to probe significant depths into the interior non-destructively. However, such facilities are few and access can be difficult to obtain. One way of assessing whether synchrotron X-rays or neutrons are well suited is to use published attenuation data as a guide, but this neglects the fact that synchrotron X-ray fluxes are many orders of magnitude greater than those typical of neutron instruments. This means that 1% transmission may be acceptable for a high-flux synchrotron X-ray source instrument but hopelessly inadequate for a neutron instrument. At the same time, large arrays of efficient detectors may offset lower incident fluxes. Conversely, high background levels may put a limit on the minimum acceptable signal. In part I of this study (Withers, 2004), a simple quantitative approach for calculating the maximum feasible path length as a function of the related experimental variables was presented. In part II, this approach is applied to examine a variety of issues of concern to those attempting to make accurate measurements of strain quickly and efficiently. It is shown that three instrumental parameters ($\Phi_{\rm instr}$, β_0 and $\beta_{\rm sample}$) can capture the essence of instrumental performance, and the use of scans into the sample in reflection is suggested as a means of deriving these parameters.

One criticism of establishing benchmark data is that the capabilities of instruments for strain measurement are not static but tend to develop over time. As a result, benchmark data accumulated for a given instrument tend to be superseded by better performances as new detectors and configurations that are more optimized are developed. This tendency does not seem to be a disadvantage; rather the acquisition of such data using calibration samples on a regular basis could be used to monitor what might otherwise be imperceptible but steady incremental improvements in performance. Besides, with the advent of dedicated strain-measurement instruments, the performance of specific instruments is becoming more repeatable and predictable. In any event, without a great deal of sample-specific information (*e.g.* texture, grain size *etc.*), the approach could not be relied upon to timetable accurately a detailed series of measurements. Instead, the method presented here provides a means of comparing different measurement strategies, delineating the broad capabilities of different instruments, and assessing the best instrument type and energy range for a given investigation, as well as providing a basis for establishing design principles for new instruments.

2. Test samples and preliminary calibration of instruments

The key to making quantitative comparisons between instruments is to establish a method for quantifying their performance. In order to do so it is important to decide on instrumental constants that can be measured at different instruments on specific calibration samples. In part I, the use of a depth scan in reflection geometry was proposed to

Table 1
Estimated maximum feasible penetration depths (in mm) for transmission and reflection geometries corresponding to the maximum path lengths given in Table 4 of part I, calculated on the basis of 1 h acquisition times for neutrons and a diffraction peak height to background ratio of 1 for synchrotron X-rays.

The value for conventional laboratory X-rays is based on the depth over which 63% of the detected signal arises.

			Al		Ti		Fe		Ni		Cu	
	θ (°)	u_θ (°)	$D_{\rm trans}$	$D_{\rm refl}$	$D_{\rm trans}$	$D_{\rm refl}$	$D_{\rm trans}$	$D_{\rm refl}$	$D_{\rm trans}$	$D_{\rm refl}$	$D_{\rm trans}$	$D_{\rm refl}$
Neutrons	45	0.147	115	55	15	10	30	15	15	7	25	13
ID31 (60 keV)	8	0.002	45	3.2	16	1.1	9	0.6	5	0.3	5	0.3
ID11 (50 keV)	8	0.004	55	3.8	13	0.9	6	0.4	3.5	0.25	3.4	0.25
BM16 (40 keV)	10	0.004	45	3.8	9	0.8	4	0.3	2.4	0.2	2.3	0.2
16.3 SRS (30 keV)	10	0.005	17	1.5	3.2	0.3	1.5	0.1	0.9	0.08	0.8	0.07
Lab. Cu X-rays	65	–		0.034		0.005		0.002		0.010		0.010

provide both diffracted signal and background data. Ideally this data would be collected for standard (reference) test samples (Withers, 2004). In part I it was shown that from such measurements it is possible to derive three instrumental calibration constants. The instrumental flux constant ($\Phi_{\rm instr}$) is the flux that would be detected on an instrument were all incident particles diffracted into a cone of scattering angle 2θ and is defined in equation (18) of part I. The total flat background, $B_{\rm tot}$, recorded for a diffraction peak measurement was taken to comprise three terms, namely a component, B_0 (= $b_0 t$), present even when the gauge volume was empty; $B_{\rm incoh}$, the incoherent contribution (for neutrons); and $B_{\rm sample}$ (= $b_{\rm sample} t$), which incorporates the remaining contributions. $B_{\rm sample}$ is equal to $B_{\rm tot} - (B_0 + B_{\rm incoh})$ and represents other sample-related contributions to the background count. B_0 has been taken to be independent of the sample, an assumption that appears to hold good for synchrotrons, but there is some evidence, especially for neutrons, that highly scattering materials give a larger background signal even when they are not within the sampling volume. B_0 and $B_{\rm sample}$ can be derived from a depth scan made in reflection geometry, as shown in Fig. 2 of part I, from which the instrumental constants β_0 and $\beta_{\rm sample}$ can be derived using equation (21) (part I). Approximate values of $\Phi_{\rm instr}$, β_0 and $\beta_{\rm sample}$ have been derived using such surface entrance scans (mostly the Al^{311} using a standard sample) at a wide range of neutron and synchrotron sources. Where this data has not been available, data collected for the VAMAS TWA20 Al shrink-fit plug round-robin study have been used (Webster, 2000).

As discussed in part I, the incident fluxes at neutron sources are 1000–10 000 times smaller than those at third-generation X-ray sources (Table 3 of part I). This difference is partially compensated for by correspondingly smaller background fluxes. Throughout the present paper, it has been assumed that neutron measurements are made for a gauge volume of 40 mm^3 and synchrotron measurements for a gauge of 1 mm^3. The synchrotron instruments studied are 16.3 (SRS Daresbury), BM16, ID11 and ID31 (at the ESRF) having energies of 30, 40, 50 and 60 keV, for which the instrumental constants are listed in Table 3 of part I. Analyser crystals were used on all X-ray instruments except station 16.3. The associated characteristic diffraction angles and peak widths are given in Table 1.

3. The maximum feasible depth

In part I (Withers, 2004), the maximum feasible path lengths were calculated for Al, Ti, Fe, Ni and Cu for a generic neutron instrument (based broadly on the Chalk River NRU LR3 instrument) and several X-ray instruments having different energies. Two criteria were proposed for defining the maximum path length: the maximum acceptable acquisition time (taken to be 1 h) and the minimum acceptable peak height to background ratio (taken to be 1), giving the path lengths l_t and $l_{h/b}$, respectively. It was suggested that the former was probably more appropriate to neutron experiments, while the latter may be more suited to synchrotron experiments. From these criteria, it is a simple matter to calculate the maximum feasible depths for simple transmission and reflection geometries for a plate.

In transmission, the maximum feasible depth ($D_{\rm trans}$) is related to the maximum path length (l_t or $l_{h/b}$) and the diffraction angle ($\theta_{\rm B}^{hkl}$) by

$$D_{\rm trans} = l_t \cos\theta_{\rm B}^{hkl}. \quad (1)$$

This value is equivalent to the maximum feasible thickness that can be probed in transmission. High penetrations are favoured by low scattering angles, such as those used in synchrotron diffraction. The maximum path lengths for neutrons and synchrotron X-rays are summarized in Table 1 and Fig. 1(*a*) on the basis that the 1 h acquisition time criterion is more appropriate for neutrons and the signal-to-background criterion is more appropriate for synchrotron X-rays. It is clear that high-energy X-ray synchrotron instruments can compete with neutrons in terms of depth penetration in transmission. Unsurprisingly, the point at which neutron sources hold an advantage moves to smaller depths with increasing atomic number and lower X-ray energy.

In reflection, the maximum feasible depth ($D_{\rm refl}$) is related to the maximum path length,

$$D_{\rm refl} = 0.5\, l_t \sin\theta_{\rm B}^{hkl}. \quad (2)$$

This geometry favours high angles for good penetration and access, such as those employed in conventional X-ray diffraction. The maximum depths are summarized in Table 1 and Fig. 1(*b*) for the engineering materials covered here. It is clear that, when using low-order *hkl* diffraction peaks, high-

energy X-rays struggle to compete with neutrons except for near-surface regions ($\lesssim 1$ mm). Little is gained by using higher energies because of the greater path lengths associated with the shallower scattering angles. One possibility at high energies is to move to higher-order reflections in order to increase the scattering angle; this alternative has not been examined quantitatively here. The thickness of a test piece that can be examined is twice $D_{\rm refl}$ provided that access is available from both surfaces of the component. For comparison, the table also includes the penetration depth for laboratory X-rays in reflection. This depth is defined differently in terms of the attenuation coefficient (μ), as the fraction (G_x) of the total intensity diffracted by a surface layer of depth x (Cullity, 1978), since conventional X-ray measurements do not typically rely on incident and diffracted slits to scan the gauge with depth:

$$G_x = \left[1 - \exp(-2\mu x/\sin\theta_{\rm B}^{hkl})\right]. \qquad (3)$$

It is clear from Table 1 that, in contrast to synchrotron X-rays and neutrons, for laboratory X-rays nearly all the diffracted signal comes from a very thin surface region.

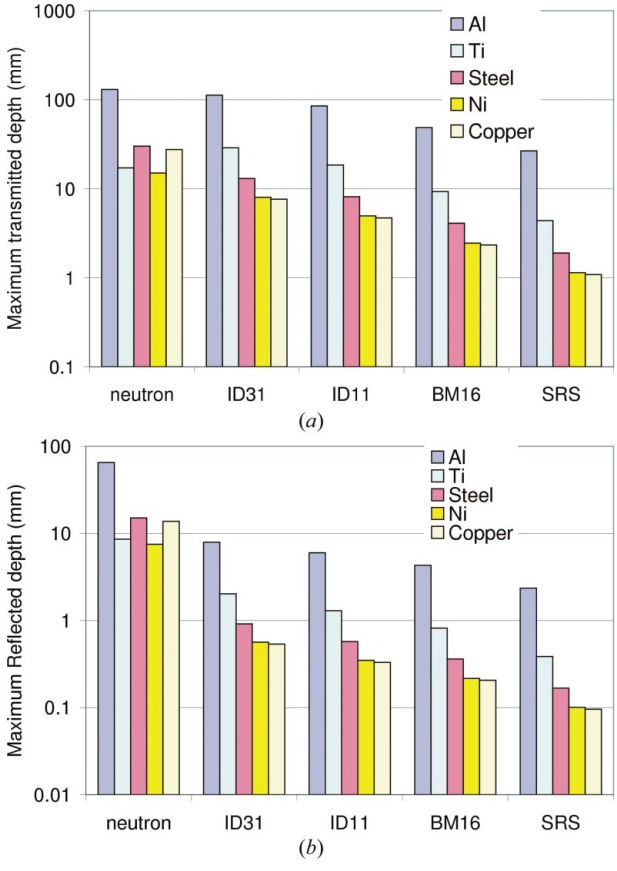

Figure 1
The maximum feasible depths for (*a*) transmission and (*b*) reflection for a generic neutron source and various synchrotron X-ray sources, based on an acquisition time of 1 h for neutron measurements, using a sampling gauge of 40 mm^3, and based on a peak to background ratio of 1 and a sampling volume of 1 mm^3 for synchrotron X-rays. Other parameters were extracted from preliminary experiments, as described in Table 1 and part I (Withers, 2004).

4. Measurements in transmission

When using the transmission geometry for the measurement of in-plane strains in plate-like samples, the path length does not vary as a function of the depth of the measurement through the plate. However, advantage can still be gained, at least for X-rays, by maximizing the diffracted count rate *via* appropriate tailoring of the attenuation coefficient to the path length through the sample. If the attenuation is too low then, while most of the incident beam will pass through the sample, little will be scattered from the gauge volume; if the attenuation is too large, little of the beam will be transmitted through the sample, giving a low diffracted signal. As a working guide it has been said that a good signal will be achieved when the attenuation length, l_μ (length over which flux reduces by 63%), is comparable with the path length ($l_\mu \simeq l$). The framework defined in part I enables an examination of the validity of this guideline.

Of course, the proportion of the incident beam that is transmitted [$P_{\rm transmit}(l)$] varies as $\exp(-\mu l)$ [equation (9), part I]. On the other hand, the probability of diffraction ($P_{\rm diff}^{hkl}$) varies as $\lambda^3\Sigma_{\rm coh}$ [equation (11), part I]. For synchrotron radiation, these terms vary in a systematic way with the X-ray energy. A graph of the number of counts expected as a function of transmitted path length and incident X-ray energy is shown in Fig. 2, for a sampling volume of 1 mm^3 of Al based on data acquired at 60 keV for the ID31 beamline at the ESRF. Normally the flux delivered by an instrument varies as a function of energy, but in order to examine the competing effects of attenuation and scattering, the incident flux has been taken to be constant and independent of energy. Note that, as expected, the maximum signal for a given sample thickness lies at intermediate energy. Unsurprisingly, the optimal energy

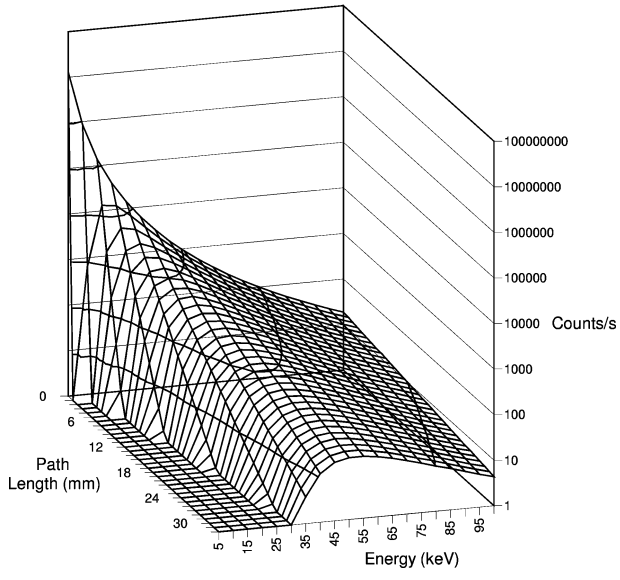

Figure 2
The number of (311) diffraction peak counts per second expected on ID31 for a 1 mm^3 gauge of Al in transmission as a function of energy and path length (sample thickness), assuming the instrumental flux to be independent of energy.

increases with sample thickness (see Fig. 3*a*). However, the largest count rate is not obtained at an energy giving a constant ratio of l/l_μ with increasing thickness. Rather, as the thickness increases, the optimal attenuation length becomes a smaller and smaller fraction of the total path length. For example, for a 5 mm Al plate the optimal energy is 28 keV, for which the X-ray attenuation length is 2.9 mm, giving a normalized path length of 1.74, whereas for a path length of 100 mm the optimal energy is approximately 80 keV, for which the attenuation length is approximately 18 mm (normalized path length of 5.4). Indeed, the optimal energy increases approximately as a function of the (distance)$^{1/3}$ in Fig. 3(*a*). Therefore, the energy should be increased to the third power with increasing sample thickness. In this respect it is interesting to note that the photoelectric cross section varies approximately as E^{-n}, where $2.5 < n < 3.5$ (Bragg & Pierce, 1914), and that this mechanism dominates the attenuation below 40 keV (Table 2 in part I); however, the relation extends to higher energies too. It is also evident from Fig. 3(*b*) that the normalized distance must increase approximately linearly with increasing thickness in order to obtain the highest count rates.

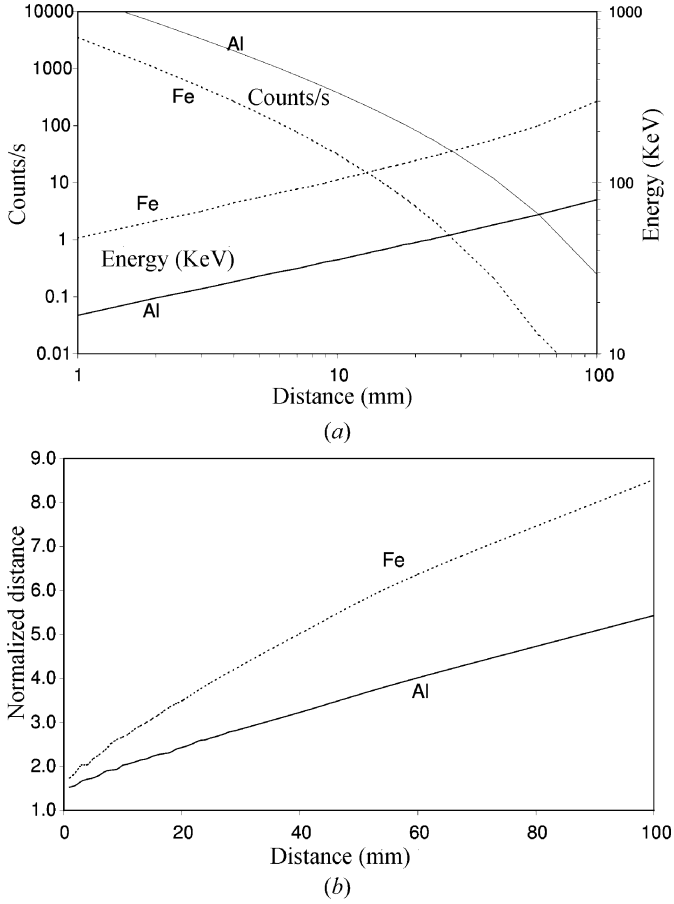

Figure 3
(*a*) The optimal energy (right-hand axis) as a function of sample thickness for Al and Fe on ID31, assuming a flux independent of energy. The corresponding count rate for a 1 mm^3 sampling gauge for (311)Al and (211)Fe expected for the optimal energy is also shown (left-hand axis). (*b*) The normalized distance (path length/attenuation length) based on the optimal energy as a function of depth.

5. Comparing the capabilities of neutron and synchrotron instruments in reflection

It is clear from the data in part I, Table 3, that both the diffracted signal and the expected background levels representative of neutron and synchrotron diffraction are different by orders of magnitude. For a neutron instrument it is common to acquire 1–10 diffracted counts per second in the diffraction peak, whereas acquisition rates of 100 or 1000 photons per second are more typical of synchrotron sources. However, that is not to say that synchrotron radiation is always preferable to neutron diffraction. The key parameter is the time needed to achieve a given strain accuracy (here taken to be 10^{-4}). The predicted times for various neutron and synchrotron sources are shown in Fig. 4 for measurements in reflection from an Al plate at a range of sampling depths using the instrumental constants given (Table 3 in part I). The figure shows clearly the time advantage of using synchrotrons for

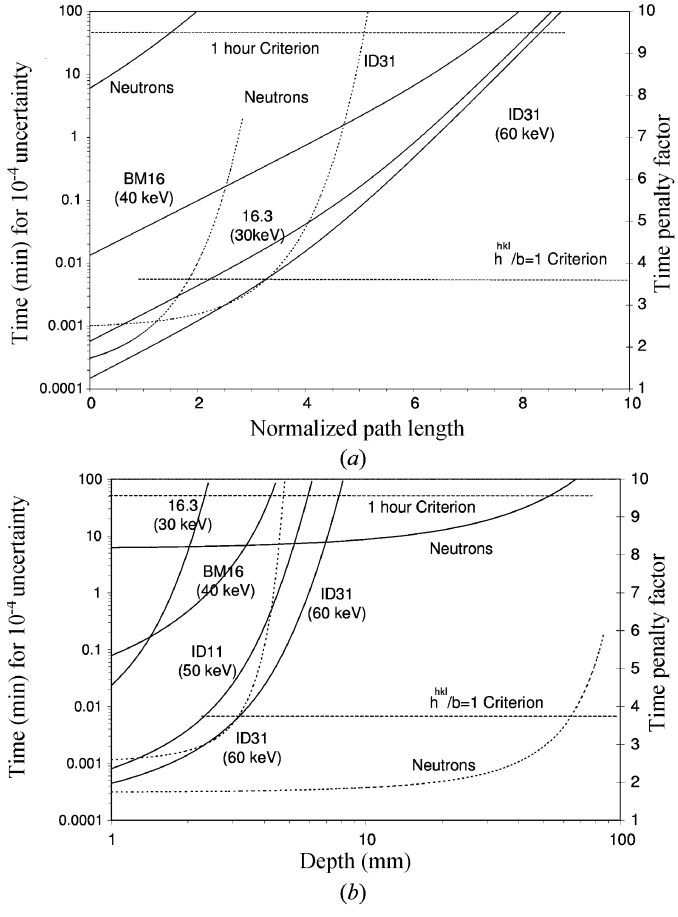

Figure 4
Acquisition times to achieve 10^{-4} strain accuracy using neutron (Chalk River L3) and various synchrotron instruments with an Al sampling gauge of 1 mm^3 for synchrotrons and 40 mm^3 for neutrons as a function of (*a*) normalized path length and (*b*) depth in reflection geometry using the angles and peak widths given in Table 4 of part I. The dashed curves show the corresponding background penalty factors $[1 + 2(2)^{1/2}b/h^{hkl}]$ for neutrons and ID31. The dashed horizontal lines delineate the 1 h (left-hand axis) and peak to background ratio of 1 maximum feasible depth criteria (right-hand axis).

near-surface measurements in light metals (below 3 mm depth).

It is clear from Fig. 4(*a*) that, as noted in part I in relation to Fig. 4, the time taken to acquire a given strain accuracy does not vary exponentially with depth. The origin of this non-linearity is due in part to the variation in the diffraction peak height to background penalty factor $[1 + 2(2)^{1/2}b/h^{hkl}]$, which characterizes the increased signal (or time) required over that needed were there no background count at all. Over depths of practical interest, the dashed curves in Fig. 4 show that the instrumental curves transfer from the negligible background limit (penalty factor in the region of 1) to the significant background limit (penalty factor $\gg 1$). Near the surface, the sample-dependent background falls in proportion to the signal (see Fig. 5 of part I) approximately exponentially with increasing depth, so that the peak height to background ratio remains approximately constant. At larger depths, the diffracted count rate and the sample-dependent background rate fall to a level at which the constant background component, b_0, becomes significant and h^{hkl}/b decreases. At these depths the deleterious effect of the penalty factor causes the lines to curve upwards steeply towards longer acquisition times.

The difference between the 1 h acquisition time limited feasibility criterion and the peak height to background ratio of 1 criterion is well illustrated in Fig. 4(*b*). For synchrotron X-ray instruments, the steepness of the curve between exceeding the h^{hkl}/b criterion and reaching the $t = 60$ min criterion is such that very modest benefits are realised in terms of the increased depth achievable for much longer acquisition times. This situation is exemplified by the data in Table 4 (part I), where the times taken to achieve the maximum depth are typically of the order of minutes ($t_{h/b}$) for the peak to background criterion, whilst accessing a depth of 50–90% of those attained in 1 h. This result confirms that, unless background levels can be seriously reduced, synchrotron instruments are suited to short (< 10 min) timescale measurements, in contrast to neutron instruments. Fig. 4(*a*) illustrates that, depending on the criteria, path lengths of between four and eight times the attenuation length are possible for instruments on third-generation synchrotron sources; path lengths of approximately two to four times the attenuation length are possible for current neutron instruments.

6. Measurements on different neutron instruments

No systematic quantitative comparison of the capability of neutron instruments worldwide has yet been undertaken. However, a number of round-robin studies have been undertaken under the auspices of the VAMAS TWA20 standardization study (Webster, 2001), from which preliminary data can be drawn. The most comprehensive has been a study of the variation of strains within an Al shrink-fit ring and plug (Webster, 2000). The performance of each individual facility has not been identified, but the range of detected flux constants, $\Phi_{\rm instr}$, and background constants characteristic of these instruments is clear from Fig. 5. Note that the rate at which diffraction peak data are acquired, h^{hkl}, varies by two orders of magnitude. Of course, incident flux is not the only important variable; the background signal is an important factor in determining the maximum depth at which a peak can practically be acquired. Unsurprisingly, on the whole, instruments with the largest diffracted peak flux also record the largest background count rates. The ratio between sample-dependent background, which does not seriously limit the maximum feasible depth, and sample-independent background is also very different from instrument to instrument. Analysis of these curves may provide pathways to improving the performance characteristics of particular instruments. The time taken to acquire a diffraction peak to 10^{-4} strain accuracy is also plotted against the right-hand axis in Fig. 5. The acquisition time is strongly dependent on the peak width as well as the detected flux; this varies by a factor of two between the instruments surveyed. Narrower peak widths also have the advantage that the peak height is greater for the same sample diffracted signal, reducing the time penalty factor. Note that the acquisition times obtained on the basis of this preliminary study cover a range of nearly three orders of magnitude. New dedicated instruments, including SMARTS at LANSCE and VULCAN at SNS (US), SALSA at the ILL (France), and ENGIN-X at ISIS (UK), for which such data are not yet available, may extend the envelope of performance further.

7. Conclusions

While the accurate prediction of measurement times for a particular previously untested sample remains some way off and would require considerable prior knowledge about the sample of interest, as well as the instrumental configuration, much can be gained by establishing a simple estimator of instrumental capabilities. In part I, such an estimator was

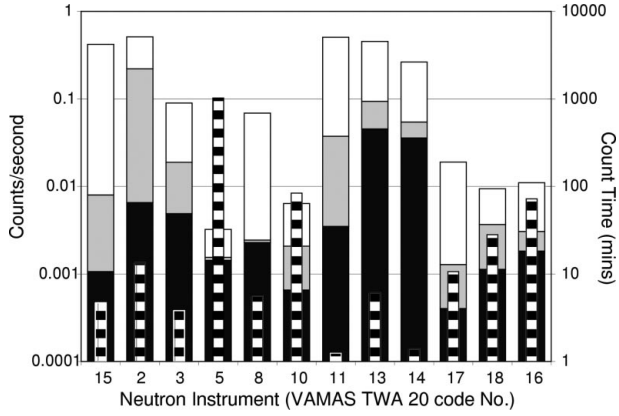

Figure 5
The peak height (h^{hkl}, white), and sample-dependent ($b_{\rm sample}$, grey) and constant background (b_0, black) count levels per second (left-hand axis), for a 40 mm^3 Al gauge volume at zero depth for many neutron instruments worldwide, based on data collected for an Al ring and plug as part of a round robin. Also shown as narrow columns are the count times to acquire to 10^{-4} strain accuracy at zero depth (right-hand axis). The instrument identifier codes correspond to those in the VAMAS TWA20 report (Webster, 2000).

developed on the basis of sound physical principles. Application of this estimator in part II has shown the following.

(i) It is possible to determine the conditions under which neutron and synchrotron instruments are cost effective. In addition, it is possible to identify the most appropriate X-ray instrument and energy for a given measurement task.

(ii) In transmission, the X-ray energy should be varied as the cube root of the sample thickness in order to achieve optimal acquisition times, all other things being equal. In practice, the variation in instrumental flux with energy must also be factored into the optimization. It should be noted that our recent experiments on ID15 on 25 mm thick steel samples at ~150 keV confirm the trends plotted in Fig. 3(*a*).

(iii) The performance of current neutron instruments is limited primarily by the peak width and detected flux; synchrotron instruments, on the other hand, are limited in depth penetration primarily by the background count. Neutron instruments can penetrate in excess of two times the attenuation length, whereas synchrotron instruments can penetrate in excess of four times the attenuation length. With good instrument design it should be possible to extend these limits considerably.

(iv) At the current time, synchrotron X-ray instruments are competitive with neutrons (provided one has access to sufficiently hard X-rays) for all transmission thicknesses, offering faster measurement times at better spatial resolutions (Fig. 1*a*). In contrast, synchrotrons are limited to the near-surface regime (< 1 mm in most cases) in reflection (Fig. 1*b*). This is an important regime technologically and one over which neutron measurements are affected by spurious surface-related effects. Their excellent acquisition rate in transmission but poor depth capability in reflection makes synchrotron X-rays well suited for two-dimensional strain mapping, but only rarely suitable for determining three-dimensional strain fields. In cases where mechanics arguments do not enable us to calculate the out-of-plane strain or stress component, it is not possible to obtain stresses solely from such two-dimensional strain maps. Researchers are already starting to combine synchrotron (in-plane) and neutron (out-of-plane) strain results to obtain stress fields cost efficiently (Stelmukh *et al.*, 2002). Furthermore, two-dimensional strain maps are an excellent means of validating FE models of process or service-induced residual stresses.

(v) This study has provided a framework for comparing the performance of existing and new instruments. A method has been proposed for obtaining calibration constants for all instruments from a simple depth scan that can be undertaken in under 1 h at most instruments. Here preliminary data have shown important variations in performance from instrument to instrument. The acquisition of such data on a well characterized 'standard' material at instruments worldwide would lead to quantitative benchmarks for monitoring and aiding the future development of our instrument portfolio and hard data on which experimenters could select optimized measurement configurations.

This paper could not have been written without the help of all those responsible for running neutron and synchrotron strain instruments worldwide. Special thanks go to Drs A. Fitch, J. Wright and M. R. Daymond for help extracting raw data, D. Hughes, A. Evans, J. Fonseca and P. A. Browne for making their experimental data available, and C. Ohms for providing data from the VAMAS TWA20 project. Helpful discussions have been had with Professor P. J. Webster and Drs M. W. Johnson, S. S. Hasnain, M. R. Daymond and A. Steuwer. Funding from the European Community, the EPSRC and a Royal Society Wolfson Merit Award is also gratefully acknowledged.

References

Bragg, W. H. & Pierce, S. E. (1914). *Philos. Mag.* **18**, 626–630.
Cullity, B. D. (1978). In *Elements of X-ray Diffraction*. Reading, MA: Addison-Wesley.
Stelmukh, V., Edwards, L., Stantisteban, J. R., Ganguly, S. & Fitzpatrick, M. E. (2002). *Mater. Sci. Forum*, **404–407**, 599–604.
Webster, G. A. (2000). *Neutron Diffraction Measurements of Residual Stress in a Shrink-Fit Ring and Plug. Versailles Project on Advanced Materials and Standards TWA20.* VAMAS Report No. 38. (ISSN 1016-2186.)
Webster, G. A. (2001). Editor. *Polycrystalline Materials – Determinations of Residual Stresses by Neutron Diffraction. ISO/TTA3 Technology Trends Assessment*. Geneva: ISO.
Withers, P. J. (2004). *J. Appl. Cryst.* **37**, 596–606.